ACS OMEGA

http://pubs.acs.org/journal/acsodf

Article

Highly Stable Polymer Coating on Silver Nanoparticles for Efficient Plasmonic Enhancement of Fluorescence

Ryo Kato, Mitsuhiro Uesugi, Yoshie Komatsu, Fusatoshi Okamoto, Takuo Tanaka, Fumihisa Kitawaki, and Taka-aki Yano*

Cite This: *ACS Omega* 2022, 7, 4286−4292

Read Online

ACCESS | Metrics & More | Article Recommendations | Supporting Information

ABSTRACT: Surface coating of plasmonic nanoparticles is of huge importance to suppress fluorescence quenching in plasmon-enhanced fluorescence sensing. Herein, a one-pot method for synthesizing polymer-coated silver nanoparticles was developed using a functional polymer conjugated with disulfide-containing anchoring groups. The disulfides played a crucial role in covalently bonding polymers to the surface of the silver nanoparticles. The covalent bond enabled the polymer layer to form a long-term stable coating on the silver nanoparticles. The polymer layer coated was adequately thin to efficiently achieve plasmonic enhancement of fluorescence and also thick enough to effectively suppress quenching of fluorescence, achieving a huge net enhancement of fluorescence. The polymer-coated plasmonic nanoparticles are a promising platform for demonstrating highly sensitive biosensing for medical diagnostics.

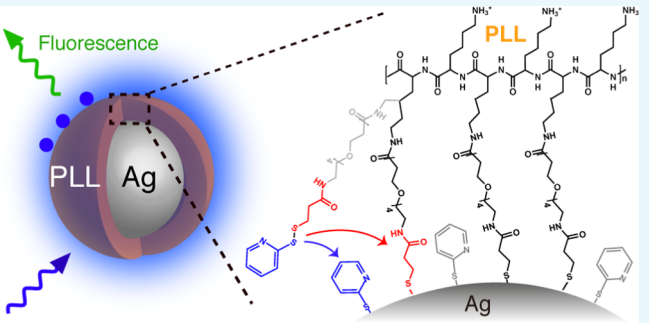

1. INTRODUCTION

Plasmon-enhanced fluorescence has attracted considerable attention in medical diagnostics owing to its capability of highly sensitive biosensing.[1−5] Localized surface plasmon resonances (LSPRs) in metallic nanoparticles induce the locally enhanced electromagnetic fields that resonantly excite molecular fluorescence near the nanoparticle. The plasmonically enhanced fluorescence increases significantly as the nanoparticle−fluorophore separation distance decreases, enabling the detection of even single-molecule fluorescence.[6,7] On the other hand, when a fluorophore stays in the close proximity of the surface of the metallic nanoparticles, nonradiative energy transfer from the fluorophore to the metal occurs crucially, resulting in quenching of the fluorescence. Depending on the spatial separation distance, there is a strong competition between the two opposite effects (i.e., nonradiative fluorescence quenching and plasmonic fluorescence enhancement effects). In particular, for a short separation distance of within 3 nm, the quenching dominates over the electromagnetic enhancement,[8,9] and therefore, the net fluorescence enhancement by the efficient suppression of the quenching effect is maximized at a distance of ∼4 nm. The maximum net enhancement of fluorescence is achieved by employing thin physical spacers to separate fluorophores from metallic nanoparticles.

Much effort has been devoted so far to introduction of antiquenching spacers. One of the most promising approaches is to use core−shell nanoparticles, where metallic (plasmonic) cores are coated with adequately thin nonmetallic shells.[4,10] Silica is most commonly utilized as a shell material because of its easy synthetic process and high controllability of thickness.[11−18] A facile chemical synthesis of silica layers on any noble metal nanoparticles has been demonstrated by many groups,[19−21] which offers versatile applications in the field of catalysis, optics, and electronics. Properties of silica core−shell nanoparticles, such as thickness and components of shell layers, can also be tunable. In recent advancement of nanotechnology, even single-atomic layer and pinhole-free core−shell nanoparticles as well as metallic nanostructures were also demonstrated, which benefits both fluorescence and surface- and tip-enhanced Raman spectroscopy.[22] Separation distance- and excitation wavelength-dependent quenching of fluorescence has been thoroughly investigated using controlled thickness of the silica shell.[23] Besides silica, other dielectric shell materials such as Al_2O_3 and ZnO have been proven to affect the quenching efficiency depending on their refractive indices.[24] Even though silica-coated metallic nanoparticles with a variety of shell thicknesses are already commercially available, it is still challenging to reproducibly control the thickness

Received: October 27, 2021
Accepted: December 28, 2021
Published: January 7, 2022

lower than 5 nm. Alkanethiol[25] and DNA[26,27] molecules are other candidates for the spacer material. Furthermore, polymer shells[28−30] possess practical advantages in terms of chemical stability, excellent compatibility in a polymer matrix, and versatility of surface modification for the conjugation of a variety of molecules including biomolecules and dyes. The polymer shells are usually formed with coupling agents and multiple steps, which requires one to properly select the coupling agents and optimize parameters. Furthermore, the stability of the polymer coating should also be improved for further use of polymer-coated plasmonic particles in a wide range of applications.

Herein, we demonstrate a one-pot method for the highly stable coating of Ag nanoparticles with a functional polymer, possessing positively charged hydrophilic amino groups. The simple mixture of the polymer solution with the Ag nanoparticles enabled the formation of polymeric shells, whose thicknesses were sufficient for suppressing fluorescence quenching. The critical roles of the disulfide sites of the functional polymer for stable polymer coatings were addressed spectroscopically. Strong plasmonic enhancement of fluorescence excitation and efficient suppression of fluorescence quenching were demonstrated using polymer-coated Ag nanoparticles.

2. MATERIALS AND METHODS

2.1. Chemicals and Reagents. All chemicals and reagents used were of analytical grade. Poly-L-lysine (PLL) hydrochloride (M.W. >12 000, cutoff by dialysis) was purchased from PEPTIDE INSTITUTE. PEGylated, long-chain SPDP cross-linker (PEG4-SPDP) and Alexa Fluor 430 NHS ester were obtained from Thermo Fisher Scientific. Citrate-coated colloidal silver nanoparticles (AgNPs) with a mean diameter of 80 nm were purchased from NanoComposix. Amino-functionalized polystyrene (PS) nanospheres with a mean diameter of 100 nm were obtained from Polysciences. Bissulfosuccinimidyl suberate (BS3) was supplied by Dojindo. Dimethyl sulfoxide (DMSO) was purchased from Fujifilm Wako Pure Chemical Corp. Tris(2,2′-bipyridyl)ruthenium(II) chloride hexahydrate, cysteamine, and (3-aminopropyl)triethoxysilane (APTES) were purchased from Tokyo Chemical Industry Co., Ltd (TCI).

2.2. Synthesis of PLL-PEG4-SPDP. A PLL solution (1 mg/mL, 4 mL) was mixed with PEG4-SPDP (10 mg/mL, 0.373 mL) dissolved in DMSO and followed by inversion mixing for 4 h at room temperature. The mixed solution was purified by centrifuging thrice at 4 °C for 45 min at 7500*g*. The resulting solution was diluted in ultrapure water, and the optical density (OD) was adjusted to 12 at 280 nm.

2.3. Surface Coating of AgNPs with PLL-PEG4-SPDP. The 80 nm AgNPs suspended in 2 mM sodium citrate were diluted in ultrapure water, and the OD was adjusted to 0.1 at 450 nm. The AgNP solution (1.6 mL) was mixed with the PLL-PEG4-SPDP solution (0.128 mL) and followed by overnight inversion mixing. The mixed solution was purified by centrifuging thrice at 4 °C for 45 min at 12 000*g*. The resulting solution was diluted in ultrapure water, and the OD was adjusted to 0.1 at 450 nm.

2.4. Functionalization of PLL-Coated Ag and PS Nanoparticles with Alexa Fluor. Alexa Fluor 430 NHS ester (10 mg/mL, 0.068 mL) dissolved in DMSO was mixed with the PLL solution (1 mg/mL, 1 mL) and followed by inversion mixing for 4 h at room temperature. The mixed solution was purified by centrifuging thrice at 4 °C for 45 min at 7500*g*. The BS3 solution (0.5 mg/mL, 100 μL) was added into the Alexa Fluor-conjugated PLL solution (0.234 mL), further mixed with the PLL-coated AgNP solution (OD = 0.1 at 450 nm, 1 mL), and followed by inversion mixing for 1 h at room temperature. The solution was purified by centrifuging thrice at 4 °C for 30 min at 12 000*g*. The functionalization of the PLL-coated AgNPs with Alexa Fluor 430 was confirmed from the appearance of fluorescence excited at a wavelength of 430 nm.

The amino-functionalized polystyrene bead solution (100 μL) was diluted with 500 μL of DMSO buffer. Then, the solution was added into the Alexa solution (10 mg/mL, 0.0234 mL) and followed by inversion mixing for 1 h at room temperature. The mixed solution was purified by centrifuging twice at 25°C for 30 min at 10 000*g* to remove the excess of fluorescent molecules.

2.5. Functionalization of Fluorescent Dye on PLL-Coated Ag Substrates, Cysteamine-Coated Ag Substrates, and APTES-Coated Glass Substrates. The PLL-PEG4-SPDP solution (0.1 mL) and the cysteamine ethanolic solution (1 mM, 0.2 mL) were dropped onto silver-deposited glass coverslips, respectively, and left for 3 h. The substrates were subsequently rinsed with ethanol. Briefly, 0.2 mL of the APTES aqueous solution (0.25 wt %) was dropped onto a cleaned glass coverslip and left for 15 min. The substrate was then rinsed with ultrapure water and baked at 100 °C for 15 min. Finally, the Alexa solution (10 μg/mL, 0.200 mL) was dropped onto the three different substrates and left for 3 h, and the dye-functionalized substrates were rinsed with ultrapure water.

2.6. Characterization. Transmission electron microscopy (TEM) images were acquired using a scanning transmission electron microscope (ARM200F, JEOL). Scanning electron microscopy (SEM) images were obtained using a field-emission SEM (S-4700, Hitachi). Absorption and fluorescence spectra were recorded with a microplate reader (infiniteM200-PRO, TECAN). Raman spectral mapping was performed using a high-speed confocal Raman microscope (Raman11, Nanophoton) with an excitation wavelength of 532 nm. Rayleigh scattering and fluorescence spectra of individual PLL-coated Ag nanoparticles dispersed on a slide glass were obtained using a homemade microspectroscopic system combined with a dark-field inverted optical microscope (IX71, Olympus), spectrometer (Isoplane160, Teledyne), and an EMCCD camera (ProEM, Teledyne). The surface potential of the nanoparticles was measured using a ζ-potential analyzer (nano-ZS, Malvern). The diameter distribution of the nanoparticles was measured using a nanoparticle imaging analyzer (Video-drop, Myriade).

2.7. Finite-Element Method (FEM) Simulation. All FEM simulations were performed using COMSOL Multiphysics software (version 5.6). The PLL-coated Ag nanoparticles were modeled to contain a Ag spherical core with a diameter of 80 nm and a PLL layer with a thickness of 4 nm. The surrounding medium was set to be air with a refractive index of 1.0. The Ag core was coated with a PLL spacer layer of 4 nm thickness. The wavelength of the incident plane wave was set to 450 nm.

3. RESULTS AND DISCUSSION

Polymer-coated Ag nanoparticles were synthesized at room temperature in a one-pot process by mixing a polymer solution

https://doi.org/10.1021/acsomega.1c06010
ACS Omega 2022, 7, 4286−4292

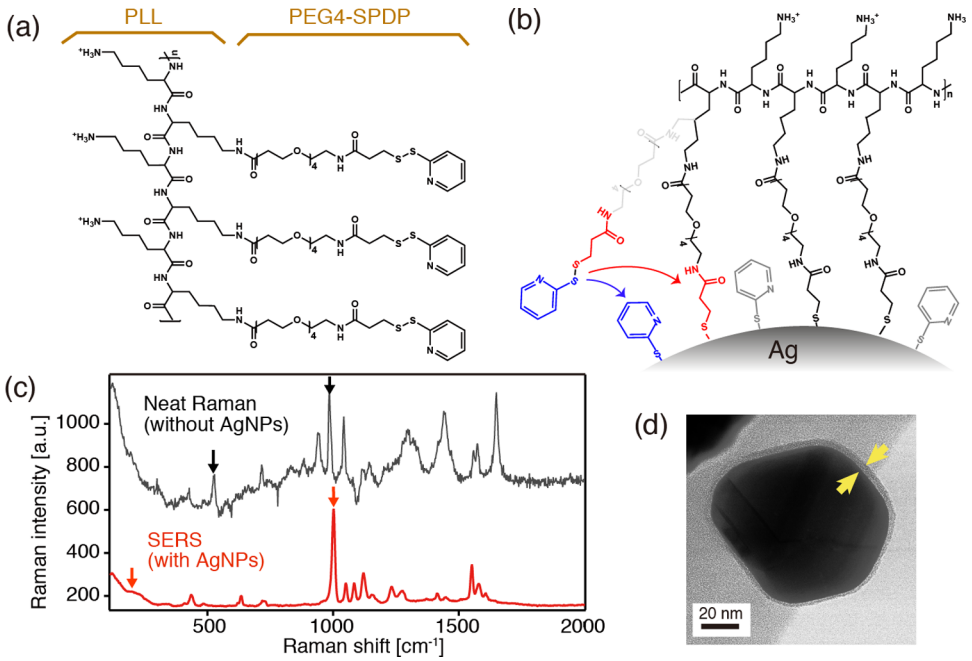

Figure 1. (a) Chemical structure of PLL in conjugation with PEG4-SPDP. (b) Schematics depicting the covalent binding of the PLL-PEG4-SPDP polymer through cleavage of disulfides. (c) Neat Raman and surface-enhanced Raman spectra of PLL-PEG4-SPDP measured with and without AgNPs, respectively. (d) TEM image of a PLL-coated core−shell nanoparticle.

with a solution of Ag nanoparticles, whose average diameter was 80 nm. The polymer used for coating the Ag nanoparticles was poly-L-lysine (PLL) conjugated with PEGylated succinimidyl 3-(2-pyridyldithio)propionate (PEG4-SPDP), and its structure is shown in Figure 1a. As schematically illustrated in Figure 1b, when the PLL-PEG4-SPDP polymers were in the close proximity to the silver surfaces of nanoparticles in the mixed solution, the disulfide bonds in SPDP were likely to be cleaved without any reducing agents such as dithiothreitol (DTT), as demonstrated earlier with other disulfide-containing reagents.[31−33] To verify the Ag-induced cleavage of the S−S bonds in our system, surface-enhanced Raman scattering (SERS) measurements were performed for the PLL-PEG4-SPDP-mixed Ag colloidal solution, as shown in Figure 1c (see Table S1 for the detailed assignment of the Raman bands). The Raman band of the S−S stretching mode at 528 cm^{-1} observed in the neat Raman spectrum of PLL-PEG4-SPDP was completely vanished in the SERS spectrum. Furthermore, a broad Ag−S stretching mode was newly appeared at around 220 cm^{-1} in the SERS spectrum. These vibrational spectroscopic signatures prove the cleavage of the S−S bonds, which initiates the linkage of the cleaved SPDP and Ag surface via the strong covalent Ag−S bond. Furthermore, the SERS spectrum exhibits a Raman band at ∼1000 cm^{-1} originating from the ring breathing mode of dissociated 2-pyridinethiol. The Raman band was slightly shifted to a higher frequency region compared to that in the neat Raman spectrum, indicating the chemisorption of 2-pyridinethiol on the Ag surface via the Ag−S bond. The chemisorbed 2-pyridinethiol induced hydrophobic interactions with the alkyl side chains of PLL, further stabilizing the linkage between PLL and Ag nanoparticles. Figure 1d shows a representative transmission electron microscopy (TEM) image of a PLL-coated Ag nanoparticle (also see another TEM image of multiple particles in Figure S1). The TEM images reveal that the nanoparticle possesses a core−shell structure with dark contrast for the Ag core with a diameter of ∼80 nm and light contrast for the PLL shell with a homogeneous thickness of ∼4 ± 1 nm, implying the successful coating of the Ag nanoparticles by PLL. The PLL shell is adequately thick to act as a spacer that prevents energy transfer between the Ag surface and fluorophores in the vicinity, leading to the effective suppression of fluorescence quenching.

Optical interferometric measurements of the nanoparticle size were performed to further verify the surface coating of the Ag nanoparticles with PLL. Figure 2a shows the diameter distributions (histograms) of the Ag nanoparticles with and

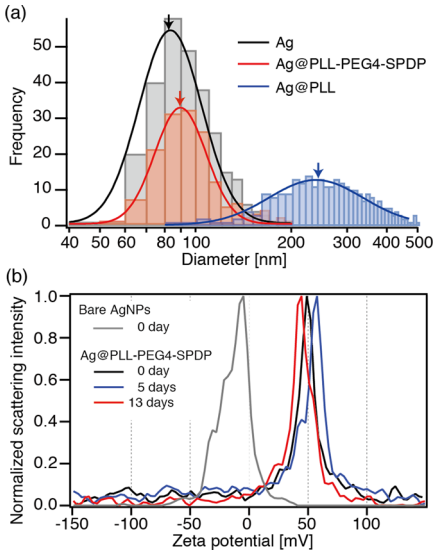

Figure 2. (a) Diameter distribution of bare Ag, Ag@PLL-PEG4-SPDP, and Ag@PLL nanoparticles, obtained by optical interferometric measurements. (b) Time-dependent ζ-potential measurements of bare Ag and Ag@PLL-PEG4-SPDP nanoparticles.

https://doi.org/10.1021/acsomega.1c06010
ACS Omega 2022, 7, 4286−4292

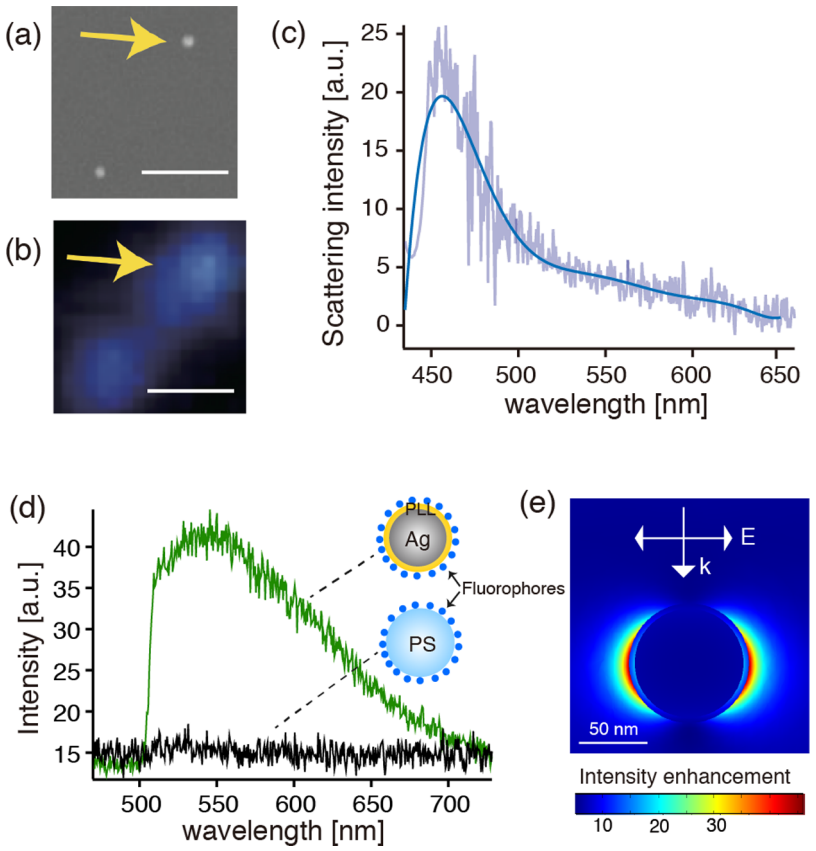

Figure 3. (a, b) SEM and dark-field optical images of the fluorophore-conjugated Ag@PLL nanoparticles dispersed on the glass substrate, respectively. The scale bars represent 1 μm. (c) Dark-field scattering spectrum of the single Ag nanoparticle indicated by the arrows in panels (a) and (b). (d) Fluorescence spectra measured on the Ag@PLL nanoparticle and the PS nanoparticles. (e) Calculated electric field distribution in the vicinity of a PLL-coated core−shell nanoparticle with a shell thickness of 4 nm and a core diameter of 80 nm, respectively, when illuminated by a plane wave of 450 nm.

without PLL coating, all of which are fitted by log-normal distribution functions to identify the mean diameter. The results revealed that the mean diameter of the Ag nanoparticles increased by ∼8 nm after the mixture of PLL-PEG4-SPDP. This indicates the formation of Ag@PLL core−shell nanoparticles with a thickness of ∼4 nm, which is consistent with the TEM observation in Figure 1d. On the other hand, when the Ag nanoparticles were mixed with PLL without conjugation of the SPDP linker, a significant increase in the size was observed along with its widened distribution, suggesting the formation of the secondary nanoparticles. This occurred because of the partial coverage of PLL on the surface of the Ag nanoparticles, which initiated the aggregation of the partially PLL-coated Ag nanoparticles. Hence, the SPDP linkers are of importance for the overall surface coverage of PLL on Ag nanoparticles.

The stability of the PLL-PEG4-SPDP coverage on the Ag nanoparticles was evaluated by ζ-potential measurements. As shown in Figure 2b, the citrate-stabilized bare Ag nanoparticles were slightly negatively charged, while the Ag@PLL-PEG4-SPDP nanoparticles possessed a highly positively charged surface immediately after the synthesis, providing high physical stability owing to the electrostatic repulsion of individual nanoparticles. The positively charged surface potential of the polymer-coated nanoparticles remained almost constant for at least 13 days after the synthesis, thereby achieving a long-term stable coverage of PLL polymers over the surface of Ag nanoparticles. These results show that the SPDP linkages play crucial roles in the stable coating of Ag nanoparticles with a homogeneous thin layer of PLL having a thickness of ∼4 nm.

To demonstrate plasmonic fluorescence enhancement using the PLL-coated Ag nanoparticles, the nanoparticles were further functionalized by fluorescent dye molecules (Alexa Fluor: λ_{ex} = 430 nm, λ_{em} = 540 nm). Figure 3a shows an SEM image of the nanoparticles monodispersed on a glass slide. Individual nanoparticles appear spatially isolated without interparticle aggregation. Figure 3b shows the corresponding dark-field optical image of the same nanoparticles, which exhibit a bright blue color originating from the LSPR of the Ag nanoparticles. Figure 3c shows the dark-field scattering spectrum of a single Ag nanoparticle, indicated by the arrows in Figure 3a,b. A distinct peak of the LSPR is observed at ∼450 nm, whose wavelength overlaps with the absorption wavelength of the fluorescent dye, enabling to plasmonically excite the dye molecules. As indicated by the green line in Figure 3d, the emission spectrum, measured on a single dye-functionalized Ag nanoparticle with the PLL coating, exhibits an obvious peak at ∼540 nm, originating from the fluorescent dye molecules functionalized over the PLL-coated Ag nanoparticle. To estimate the plasmonic enhancement factor of the fluorescence, another fluorescence spectrum was measured as a reference on a single dye-functionalized polystyrene (PS) nanosphere with a diameter of 100 nm. As the PS nanoparticles did not have any electromagnetic resonances in the visible region, fluorescence from the dye-functionalized PS nanoparticles was too weak to be detected as shown by the

https://doi.org/10.1021/acsomega.1c06010
ACS Omega 2022, 7, 4286−4292

black line in Figure 3d. Given that the fluorescence intensity from the PS nanoparticle is assumed to be the noise level of the spectrum, the fluorescence intensity ratio between the Ag and PS nanoparticles is estimated to be at least 20 times. Considering the difference in the surface area (i.e., diameter) between the Ag and PS nanoparticles, the fluorescence enhancement factor of the single PLL-coated Ag nanoparticles was estimated to be at least 26 times. To verify the plasmonic fluorescence enhancement of our polymer-coated nanoparticles, a numerical simulation was performed to estimate the electromagnetic intensity enhancement of the incident light in the vicinity of a Ag@PLL core−shell nanoparticle with a core diameter of 80 nm and a shell thickness of 4 nm. Figure 3e shows the spatial distribution of the intensity enhancement around the nanoparticle under the incidence of a plane wave with an excitation wavelength of 450 nm corresponding to the LSPR of the Ag nanoparticle. Even with the 4 nm thick layer of PLL covering the Ag nanoparticle, a strongly enhanced field is distributed on the outermost surface of the PLL layer. The maximum intensity enhancement on the outermost surface reaches 36 times, which is comparable to the experimentally obtained fluorescence enhancement. Such a high fluorescence enhancement is achievable with the use of the PLL-coated Ag nanoparticles. We would like to note here that the distributions of the electric field in the vicinity of the polymer-coated Ag nanoparticles at an off-resonant wavelength of 500 nm and with different shell thicknesses were also numerically investigated, as shown in Figure S2.

In addition to the fluorescence enhancement capability of the PLL-coated silver nanoparticles, the effect of the PLL layer on the suppression of fluorescence quenching was also investigated. Fluorescence measurements were performed on smooth Ag thin films rather than Ag nanoparticles. Due to the lack of LSPR on the smooth Ag surface, the plasmonic enhancement effect of fluorescence was excluded, enabling us to probe only the fluorescence quenching. The fluorescent dyes (Alexa 430 NHS-ester) were uniformly functionalized on the PLL-coated Ag thin films by the coupling reaction with the amino group of PLL. To measure quenching-free fluorescence as a reference, the fluorescent dyes were also functionalized on APTES-coated glass (i.e., nonmetallic) substrates by the same coupling reaction. Furthermore, the fluorescence intensity of the dyes functionalized on the cysteamine-coated Ag thin film was also measured to confirm that the quenching effect of Ag films was dominated by the separation distance between the fluorescent dyes and Ag films, since the thickness of the PLL layer and the cysteamine layer is ∼4 and 0.3 nm, respectively. Figure 4 shows the fluorescence intensity of the dye functionalized on the APTES-coated glass substrate, the PLL-coated Ag thin film, and the cysteamine-coated Ag thin film. The fluorescence signal with the PLL-coated Ag thin film quenched down to ∼20% but was still detectable owing to the suppression of the quenching effect of metals while the fluorescence signal with the cysteamine-coated Ag film quenched more significantly because of nonradiative energy transfer, which agreed with the previously reported distance dependence of fluorescence quenching in plasmonic nanoparticles.[9,23] It should be noted that the number of the binding sites for NHS-modified dye molecules on the three substrates was similar, as the coverage rate of amino groups of cysteamine and APTES molecule bindings on the metal surface was previously investigated.[34,35] The coverage rate of amino groups of the PLL-SPDP anchoring group was also estimated by taking the molecular structure into account. The present results validate the critical role of PLL-coated silver nanoparticles in the efficient suppression of fluorescence quenching, leading to the large net enhancement of the fluorescence signal.

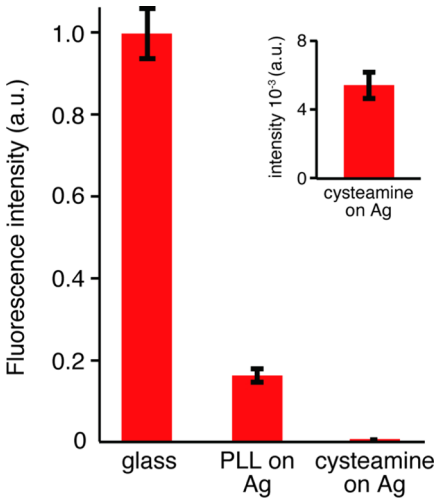

Figure 4. Fluorescence intensity of the dye Alexa 430 NHS-ester functionalized on the APTES-coated glass substrate, the PLL-coated Ag substrate, and the cysteamine-coated Ag substrate. The fluorescence signal was measured at different several locations in the samples, and the averaged fluorescence intensity was shown as the red bars and the standard deviation of the fluorescence signal was indicated as the error bars. The inset shows an enlarged graph of the fluorescence intensity of the cysteamine-coated Ag substrate.

4. CONCLUSIONS

In conclusion, a one-pot methodology for synthesizing polymer-coated plasmonic nanoparticles was developed using a functional PLL polymer conjugated with disulfide-containing anchoring groups. The disulfides played a crucial role in covalently bonding PLL polymers to the surface of the Ag nanoparticles. The covalent bond enabled the PLL layer to form a long-term stable coating on the Ag nanoparticles. The ζ-potential measurement proved that the PLL formed a positively charged polymer layer around the nanoparticles, preventing their interparticle aggregation. The shell of the PLL layer was thick enough to effectively suppress quenching of fluorescence and was also thin enough to efficiently produce plasmonic enhancement of fluorescence, thereby maximizing the net enhancement of fluorescence in the vicinity of the PLL-coated Ag nanoparticles. The enhancement of the fluorescence intensity in the vicinity of metallic nanoparticles would enable us to detect a tiny amount of fluorescent probes in biological samples with high sensitivity compared to conventional optical microscopic methods. Further, since PLL provides versatility in surface modification for the conjugation of a variety of dye-labeled biomolecules, PLL-coated plasmonic nanoparticles are a promising platform for demonstrating highly sensitive biosensing for medical diagnostics and bioimaging, such as live-cell imaging. A combination of the nanoparticle tracking system in a cell with our developed polymer-coated metallic nanoparticles with fluorescent probes would pave the way for the analysis of cellular dynamics with high spatial and temporal resolution.

https://doi.org/10.1021/acsomega.1c06010
ACS Omega 2022, 7, 4286−4292

■ ASSOCIATED CONTENT

Supporting Information

The Supporting Information is available free of charge at https://pubs.acs.org/doi/10.1021/acsomega.1c06010.

Table for assignment of Raman bands of SPDP-PLL anchoring molecules and additional simulation results of the field distribution of polymer-coated Ag nanoparticles (PDF)

■ AUTHOR INFORMATION

Corresponding Author

Taka-aki Yano − *Institute of Post-LED Photonics, Tokushima University, Tokushima 770-8506, Japan;* orcid.org/0000-0003-0063-6407; Email: yano.takaaki@tokushima-u.ac.jp

Authors

Ryo Kato − *Institute of Post-LED Photonics, Tokushima University, Tokushima 770-8506, Japan*

Mitsuhiro Uesugi − *PHC Corporation, Toon, Ehime 791-0395, Japan*

Yoshie Komatsu − *PHC Corporation, Toon, Ehime 791-0395, Japan*

Fusatoshi Okamoto − *PHC Corporation, Toon, Ehime 791-0395, Japan*

Takuo Tanaka − *Institute of Post-LED Photonics, Tokushima University, Tokushima 770-8506, Japan;* orcid.org/0000-0001-5714-5401

Fumihisa Kitawaki − *PHC Corporation, Toon, Ehime 791-0395, Japan*

Complete contact information is available at: https://pubs.acs.org/10.1021/acsomega.1c06010

Notes

The authors declare no competing financial interest.

■ ACKNOWLEDGMENTS

This research was supported by JST COI-NEXT (Grant No. JPMJPF2011), JST FOREST (Grant No. JPMJFR202I (T.Y.)), and JST ACT-X (Grant No. JPMJAX21B4 (R.K.)). The authors also acknowledge the financial support from the project on the Promotion of Regional Industries and Universities by the Cabinet Office, and the Plan for Industry Promotion and Young People's Job Creation by the Creation and Application of Next-Generation Photonics by Tokushima Prefecture.

■ REFERENCES

(1) Zhu, Z.; Yuan, P.; Li, S.; Garai, M.; Hong, M.; Xu, Q. H. Plasmon-Enhanced Fluorescence in Coupled Nanostructures and Applications in DNA Detection. *ACS Appl. Bio Mater.* **2018**, *1*, 118−124.

(2) You, Y.; Song, Q.; Wang, L.; Niu, C.; Na, N.; Ouyang, J. Silica-Coated Triangular Gold Nanoprisms as Distance-Dependent Plasmon-Enhanced Fluorescence-Based Probes for Biochemical Applications. *Nanoscale* **2016**, *8*, 18150−18160.

(3) Shrivastav, A. M.; Cvelbar, U.; Abdulhalim, I. A Comprehensive Review on Plasmonic-Based Biosensors Used in Viral Diagnostics. *Commun. Biol.* **2021**, *4*, No. 70.

(4) Zhang, Y.-J.; Radjenovic, P. M.; Zhou, X. S.; Zhang, H.; Yao, J. L.; Li, J. F. Plasmonic Core−Shell Nanomaterials and Their Applications in Spectroscopies. *Adv. Mater.* **2021**, *33*, No. 2005900.

(5) Li, J. F.; Li, C. Y.; Aroca, R. F. Plasmon-Enhanced Fluorescence Spectroscopy. *Chem. Soc. Rev.* **2017**, *46*, 3962−3979.

(6) Khatua, S.; Paulo, P. M. R.; Yuan, H.; Gupta, A.; Zijlstra, P.; Orrit, M. Resonant Plasmonic Enhancement of Single-Molecule Fluorescence by Individual Gold Nanorods. *ACS Nano* **2014**, *8*, 4440−4449.

(7) Yuan, H.; Khatua, S.; Zijlstra, P.; Yorulmaz, M.; Orrit, M. Thousand-Fold Enhancement of Single-Molecule Fluorescence near a Single Gold Nanorod. *Angew. Chem., Int. Ed.* **2013**, *52*, 1217−1221.

(8) Kühn, S.; Håkanson, U.; Rogobete, L.; Sandoghdar, V. Enhancement of Single-Molecule Fluorescence Using a Gold Nanoparticle as an Optical Nanoantenna. *Phys. Rev. Lett.* **2006**, *96*, No. 113002.

(9) Anger, P.; Bharadwaj, P.; Novotny, L. Enhancement and Quenching of Single-Molecule Fluorescence. *Phys. Rev. Lett.* **2006**, *96*, No. 017402.

(10) Huang, Y. F.; Ma, K. H.; Kang, K.; Zhao, M.; Zhang, Z. L.; Liu, Y. X.; Wen, T.; Wang, Q.; Qiu, W. Y.; Qiu, D. Core-Shell Plasmonic Nanostructures to Fine-Tune Long "Au Nanoparticle-Fluorophore" Distance and Radiative Dynamics. *Colloids Surf., A* **2013**, *421*, 101−108.

(11) Jana, N. R.; Earhart, C.; Ying, J. Y. Synthesis of Water-Soluble and Functionalized Nanoparticles by Silica Coating. *Chem. Mater.* **2007**, *19*, 5074−5082.

(12) He, H.; Muhammad, P.; Guo, Z.; Peng, Q.; Lu, H.; Liu, Z. Controllably Prepared Molecularly Imprinted Core-Shell Plasmonic Nanostructure for Plasmon-Enhanced Fluorescence Assay. *Biosens. Bioelectron.* **2019**, *146*, No. 111733.

(13) Yuan, K.; Qin, R.; Yu, J.; Li, X.; Li, L.; Yang, X.; Yu, X.; Lu, Z.; Zhang, X.; Liu, H. Effects of Localized Surface Plasmon Resonance of Ag Nanoparticles on Luminescence of Carbon Dots with Blue, Green and Yellow Emission. *Appl. Surf. Sci.* **2020**, *502*, No. 144277.

(14) Wang, L.; Song, Q.; Liu, Q.; He, D.; Ouyang, J. Plasmon-Enhanced Fluorescence-Based Core-Shell Gold Nanorods as a Near-IR Fluorescent Turn-On Sensor for the Highly Sensitive Detection of Pyrophosphate in Aqueous Solution. *Adv. Funct. Mater.* **2015**, *25*, 7017−7027.

(15) Ribeiro, T.; Baleizão, C.; Farinha, J. P. S. Artefact-Free Evaluation of Metal Enhanced Fluorescence in Silica Coated Gold Nanoparticles. *Sci. Rep.* **2017**, *7*, No. 2440.

(16) Camacho, S. A.; Aoki, P. H. B.; Albella, P.; Oliveira, O. N.; Constantino, C. J. L.; Aroca, R. F. Increasing the Enhancement Factor in Plasmon-Enhanced Fluorescence with Shell-Isolated Nanoparticles. *J. Phys. Chem. C* **2016**, *120*, 20530−20535.

(17) Cheng, D.; Xu, Q. H. Separation Distance Dependent Fluorescence Enhancement of Fluorescein Isothiocyanate by Silver Nanoparticles. *Chem. Commun.* **2007**, *3*, 248−250.

(18) Naiki, H.; Masuhara, A.; Masuo, S.; Onodera, T.; Kasai, H.; Oikawa, H. Highly Controlled Plasmonic Emission Enhancement from Metal-Semiconductor Quantum Dot Complex Nanostructures. *J. Phys. Chem. C* **2013**, *117*, 2455−2459.

(19) Tovmachenko, O. G.; Graf, C.; Van Den Heuvel, D. J.; Van Blaaderen, A.; Gerritsen, H. C. Fluorescence Enhancement by Metal-Core/Silica-Shell Nanoparticles. *Adv. Mater.* **2006**, *18*, 91−95.

(20) Caruso, F.; Spasova, M.; Salgueiriño-Maceira, V.; Liz-Marzán, L. M. Multilayer Assemblies of Silica-Encapsulated Gold Nanoparticles on Decomposable Colloid Templates. *Adv. Mater.* **2001**, *13*, 1090−1094.

(21) Pérez-Juste, J.; Correa-Duarte, M. A.; Liz-Marzán, L. M. Silica Gels with Tailored, Gold Nanorod-Driven Optical Functionalities. *Appl. Surf. Sci.* **2004**, *226*, 137−143.

(22) Huang, Y. P.; Huang, S. C.; Wang, X. J.; Bodappa, N.; Li, C. Y.; Yin, H.; Su, H. S.; Meng, M.; Zhang, H.; Ren, B.; Yang, Z. L.; Zenobi, R.; Tian, Z. Q.; Li, J. F. Shell-Isolated Tip-Enhanced Raman and Fluorescence Spectroscopy. *Angew. Chem., Int. Ed.* **2018**, *57*, 7523−7527.

(23) Reineck, P.; Gómez, D.; Ng, S. H.; Karg, M.; Bell, T.; Mulvaney, P.; Bach, U. Distance and Wavelength Dependent Quenching of Molecular Fluorescence by Au@SiO2 Core-Shell Nanoparticles. *ACS Nano* **2013**, *7*, 6636−6648.

(24) Sun, S.; Rasskazov, I. L.; Carney, P. S.; Zhang, T.; Moroz, A. Critical Role of Shell in Enhanced Fluorescence of Metal-Dielectric Core-Shell Nanoparticles. *J. Phys. Chem. C* **2020**, *124*, 13365−13373.
(25) Jana, J.; Aditya, T.; Ganguly, M.; Mehetor, S. K.; Pal, T. Fluorescence Enhancement via Varied Long-Chain Thiol Stabilized Gold Nanoparticles: A Study of Far-Field Effect. *Spectrochim. Acta, Part A* **2018**, *188*, 551−560.
(26) Chatterjee, S.; Lee, J. B.; Valappil, N. V.; Luo, D.; Menon, V. M. Investigating the Distance Limit of a Metal Nanoparticle Based Spectroscopic Ruler. *Biomed. Opt. Express* **2011**, *2*, 1727−1733.
(27) Cheng, Y.; Stakenborg, T.; Van Dorpe, P.; Lagae, L.; Wang, M.; Chen, H.; Borghs, G. Fluorescence near Gold Nanoparticles for DNA Sensing. *Anal. Chem.* **2011**, *83*, 1307−1314.
(28) Bian, Y.; Liu, S.; Zhang, Y.; Liu, Y.; Yang, X.; Lou, S.; Wu, E.; Wu, B.; Zhang, X.; Jin, Q. Distance-Dependent Plasmon-Enhanced Fluorescence of Submonolayer Rhodamine 6G by Gold Nanoparticles. *Nanoscale Res. Lett.* **2021**, *16*, No. 90.
(29) Zhang, J.; Ma, N.; Tang, F.; Cui, Q.; He, F.; Li, L. PH- and Glucose-Responsive Core-Shell Hybrid Nanoparticles with Controllable Metal-Enhanced Fluorescence Effects. *ACS Appl. Mater. Interfaces* **2012**, *4*, 1747−1751.
(30) Marsich, L.; Bonifacio, A.; Mandal, S.; Krol, S.; Beleites, C.; Sergo, V. Poly-L-Lysine-Coated Silver Nanoparticles as Positively Charged Substrates for Surface-Enhanced Raman Scattering. *Langmuir* **2012**, *28*, 13166−13171.
(31) Lee, H.; Kim, M. S.; Suh, S. W. Raman Spectroscopy of Sulphur-containing Amino Acids and Their Derivatives Adsorbed on Silver. *J. Raman Spectrosc.* **1991**, *22*, 91−96.
(32) Li, F.; Zhang, B.; Li, X.; Qiao, J.; Li, G. Effect of Different Silver Substrate on the SERS Signal of Sulfide Adsorbent. *J. Raman Spectrosc.* **2004**, *35*, 1−3.
(33) López-Tobar, E.; Hernández, B.; Ghomi, M.; Sanchez-Cortes, S. Stability of the Disulfide Bond in Cystine Adsorbed on Silver and Gold Nanoparticles as Evidenced by SERS Data. *J. Phys. Chem. C* **2013**, *117*, 1531−1537.
(34) Moon, J. H.; Shin, J. W.; Kim, S. Y.; Park, J. W. Formation of Uniform Aminosilane Thin Layers: An Imine Formation to Measure Relative Surface Density of the Amine Group. *Langmuir* **1996**, *12*, 4621−4624.
(35) Zhang, J.; Bilic, A.; Reimers, J. R.; Hush, N. S.; Ulstrup, J. Coexistence of Multiple Conformations in Cysteamine Monolayers on Au(111). *J. Phys. Chem. B* **2005**, *109*, 15355−15367.

https://doi.org/10.1021/acsomega.1c06010
ACS Omega 2022, 7, 4286−4292